Budker Institute of Nuclear Physics
SB RAS

A.V. Aleksandrov, M.S. Avilov, A.V.Antoshin,
P.A. Bak, O.Yu. Bazhenov, Yu.M. Boilmelshtein,
R.Kh. Galimov, K.V. Gubin, N.S. Dikansky,
A.G. Igolkin, I.V. Kazarezov, V.E. Carlin, N.A. Kisileva,
S.N. Klyushchev, O.V. Koroznikov, A.N. Kosarev,
N.Kh. Kot, D.E. Kuklin, A.D. Lisitsin, P.V. Logatchev,
L.A. Mironenko, A.V. Novokhatski, V.M. Pavlov,
I.L. Pivovarov, A.M. Rezakov, V.S. Severilo,
Yu.I. Semenov, B.A. Skarbo, A.N. Skrinsky,
D.P. Sukhanov, Yu.F. Tokarev, A.V. Filippov,
A.R. Frolov, V.D. Khambikov, A.N. Sharapa,
A.V. Shemyakin, S.V. Shiyankov

TEST OF THE PROTOTYPE OF VEPP-5 PREINJECTOR

Budker INP 97-98

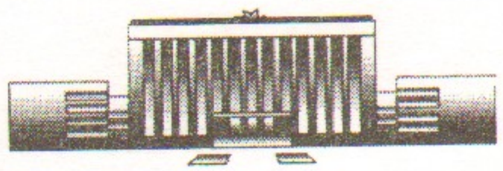

Novosibirsk

Test of the prototype of VEPP-5 preinjector

A.V. Aleksandrov, M.S. Avilov, A.V. Antoshin, P.A. Bak,
O.Yu. Bazhenov, Yu.M. Boilmelshtein, R.Kh. Galimov, K.V. Gubin,
N.S. Dikansky, A.G. Igolkin, I.V. Kazarezov, V.E. Carlin,
N.A. Kisileva, S.N. Klyushchev, O.V. Koroznikov, A.N. Kosarev,
N.Kh. Kot, D.E. Kuklin, A.D. Lisitsin, P.V. Logatchev,
L.A. Mironenko, A.V. Novokhatski, V.M. Pavlov, I.L. Pivovarov,
A.M. Rezakov, V.S. Severilo, Yu.I. Semenov, B.A. Skarbo,
A.N. Skrinsky, D.P. Sukhanov, Yu.F. Tokarev, A.V. Filippov,
A.R. Frolov, V.D. Khambikov, A.N. Sharapa, A.V. Shemyakin, S.V. Shiyankov.

Budker INP,
630090 Novosibirsk, Russian Federation.

Abstract

This work presents the results of the basic tests of VEPP-5 preinjector with 2.5-meter-long accelerating section. The main elements of the preinjector were tested at the operating condition. The average accelerating rate were up to 17 MeV/m with total beam intensity up to $1.2 \cdot 10^{10}$ particles per bunch.

Introduction

The prototype of VEPP-5 preinjector for Φ and c-τ factories [1,2] was created in order to perform the general tests of the accelerator elements. It represents an initial part of a preinjector and consist of (see fig.1): a 100 keV thermionic electron gun, an RF module on the basis of klystron KIU-12, a subharmonic buncher, a pulse compression system, an S-band bunching section, an accelerating section, a beam transport system and system of beam monitoring and control.

This article presents the basic results of the prototype tests with the 2.5-meter-long accelerating section. The average accelerating rate of an electron beam up to 17 MeV/m was achieved with up to $1.2 \cdot 10^{10}$ particles per pulse accelerated. The subharmonic buncher was not used during the presented set of experiments.

High-voltage thermionic gun

The electron bunch is produced by the 100 keV thermionic gun [3]. The basic output parameters of the gun are presented in tab. 1.

Output energy of the electron beam	100 keV
Current pulse length (FWHM)	2.5 ns
Number of electrons per pulse	$5 \cdot 10^{10}$
Repetition rate	Up to 50 Hz

Table 1: The basic parameters of the electron gun.

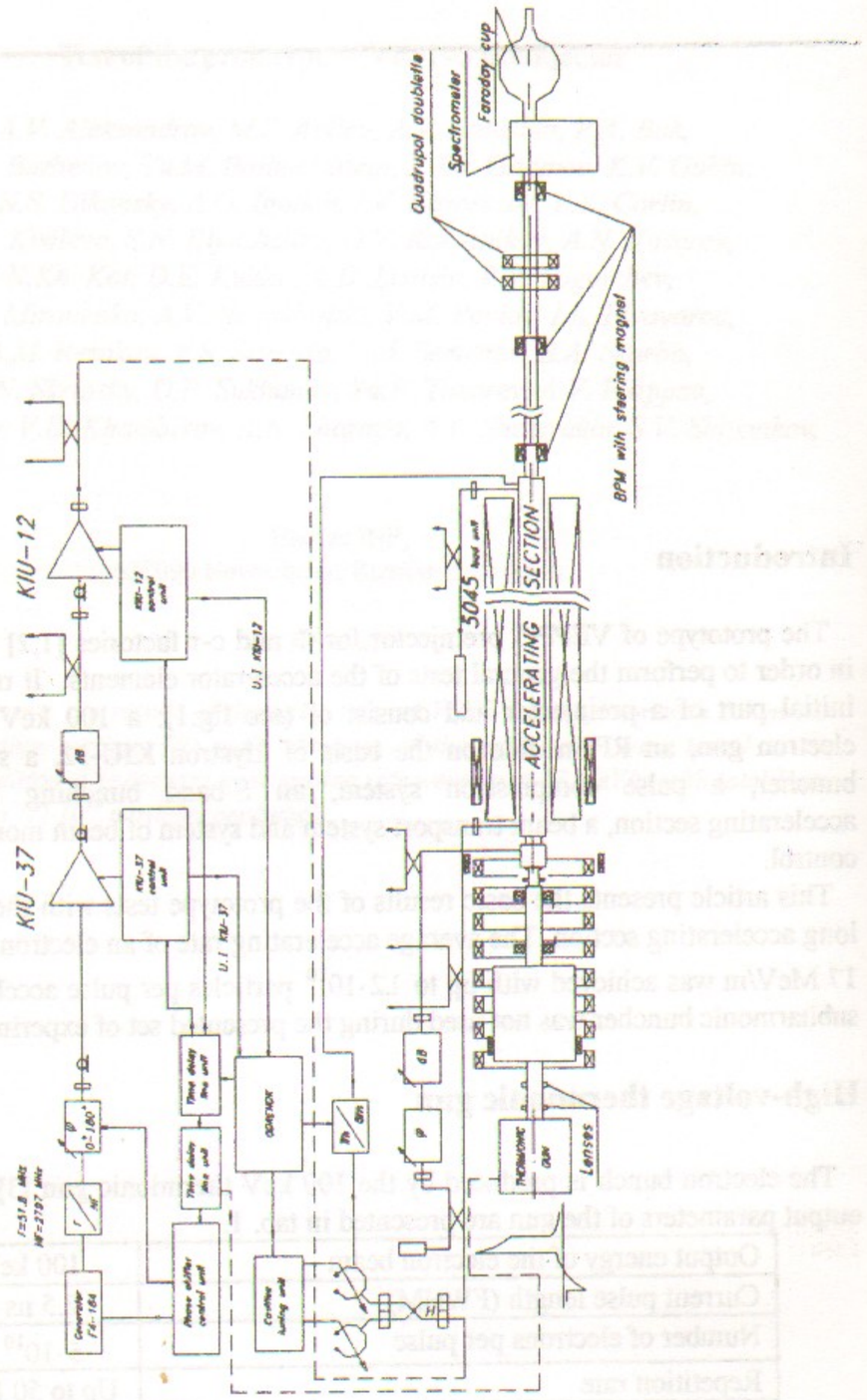

Fig. 1 The general layout of the preinjector prototype.

An RF system of the prototype

The continuous RF signal ($f \approx 51.8$ MHz, U=100 mV) from master oscillator G4-164 comes through the frequency upconverter to the step controlled 180° phase shifter. Then it is amplified by the sub-klystron KIU-37 which drives the klystron KIU-12. After KIU-12 the RF pulse of 2.5 mks length is transmitted to the SLED type pulse compression system by the evacuated waveguide (72×34 mm^2). From the output of the SLED compressor the RF pulse comes to the input of the accelerating section (AS). AS is terminated by the high power RF load. The part of the power after SLED is coupled off by the directional coupler ($\alpha_{coup} = 28$ dB) to the RF buncher. Remotely-controlled attenuator and phase shifter are used to adjust the amplitude and the phase of RF pulse at the buncher input. For the RF control the following signals are monitored by means of the directional couplers:

The amplitude of the forward signal after KIU-37,

The amplitudes of the forward and reflected signals after KIU-12 (before pulse compression system),

The amplitudes of the forward and reflected signals at the input of the RF-buncher,

The amplitudes of the forward and reflected signals at the input of the AS,

The relative phase shift between the AS input signal and the buncher input signal,

The RF power at the input of the high power load.

The pulse compression system SLED consists of the 3dB coupler and two cylindrical cavities with high Q, operating in the TE_{015} mode. The fine tuning of the cavities is performed by deformation of one of the cavity walls with the help of the step motor. The results of the cold tests of the cavities are presented in tab.2. Such parameters of the cavities were chosen to provide the quasi constant gradient along the AS when it is powered by the RF pulse after SLED system.

Diameter of cavities D	196 mm
Height of cavities h	359.7 mm
Operating frequency f_0	2797 MHz
Tune range Δf	$\pm$ 5 MHz
Frequency variation against the height of cavities variation $\Delta f/\Delta h$	2.75 MHz/mm
Unloaded quality factor Q_0	105000
Coupling factor with an incoming waveguide β	5.7
Unloaded time of the resonator $\tau_0 = Q_0 / \pi f_0$	11.9 mks
Loaded time of the resonator $T_c = \tau_0 / (1+\beta)$	1.78 mks

Table 2: Parameters of the pulse compression system SLED.

From the real pulse shape $V(t)$ after SLED system (see fig. 2) it is possible to evaluate energy consumption in the prototype elements. At the KIU-12 pulse power $P_0 \approx 13.8$ MW, pulse length $\tau_{kl} \approx 2.5$ mks, with 180° phase switch at the moment t=0, and repetition rate F=50 Hz one has:

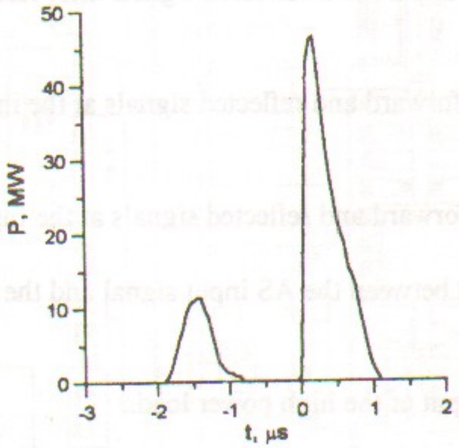

Fig. 2 An RF pulse after pulse compression system SLED.

RF energy from KIU-12 per pulse

$$W_{kl} = 34.4 \text{ J}.$$

RF energy at the AS input before phase switching

$$W_1 = \int_{-\infty}^{0} |V(t)|^2 \, dt = 4.9 \text{ J}.$$

RF energy at the AS input after phase switching

$$W_2 = \int_{0}^{\infty} |V(t)|^2 \, dt = 26.5 \text{ J}.$$

Total RF energy at the AS input during the single pulse

$$W_{acc} = W_1 + W_2 = 31.4 \text{ J}.$$

Losses in the power compression system cavities

$$W_{res} = W_{kl} - W_{acc} = 2.9 \text{ J}.$$

Average RF power from KIU-12

$$P_{kl} = W_{kl} \cdot F = 1.72 \text{ kW}.$$

Average RF power, at the input of the AS

$$P_{acc} = W_{acc} \cdot F = 1.57 \text{ kW}.$$

Average RF power, dissipated in the SLED cavities

$$P_{res} = W_{res} \cdot F = 0.145 \text{ kW}.$$

The estimations of average energy consumption have been taken into account to choose the cooling condition of the AS, the RF load and the SLED cavities.

S-band bunching section

Fig. 3 shows the details of the S-band bunching section.

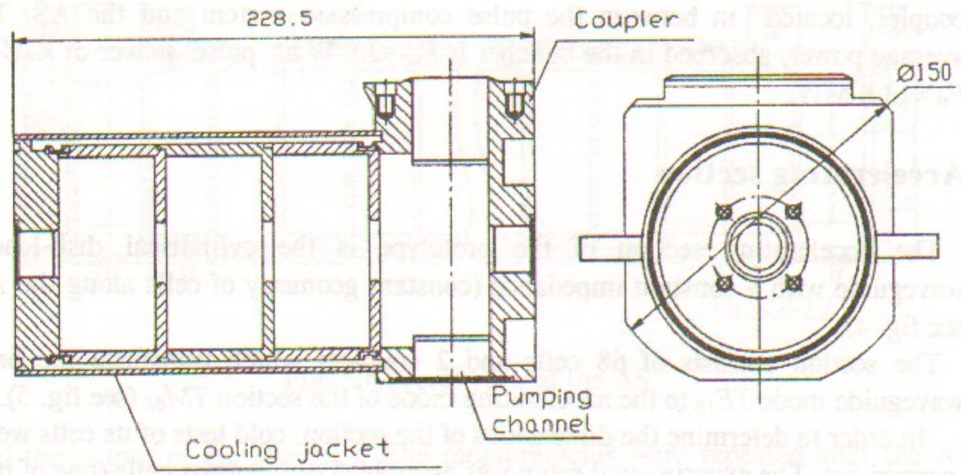

Fig. 3 Geometry of the S-band buncher.

It consists of four coupled cylindrical cavities (3 cells + 1 coupler) and operates in the $\theta = -4\pi / 3$ mode. The bunching section is made of stainless steel in order to increase the power dissipation. Therefore the bunching occurs in the increasing electric field. The bunching section has the water cooling jacket. The pumping is carried out through a pumping port located opposite to the RF power port of the coupler, that allows resolve the asymmetry problem of the coupler. The characteristics of the buncher are presented in table 3.

Diameter of a cell 2b	84.2 mm
Iris diameter 2a	24.3 mm
Iris thickness t	5 mm
Period D	39.2 mm
Resonant frequencies: f_1	2764 MHz
f_2	2778 MHz
(operating frequency) $f_{0b}=f_3$	2797.71 MHz
f_4	2811 MHz
Unloaded quality factor at operating frequency Q_{0b}	980
Coupling factor of the buncher at operating frequency β_b	1.44
Unloaded time at operating frequency $\tau_{0b}=2Q_{0b}/\omega_{0b}$	0.112 mks

Table 3: Parameters of the RF-buncher.

The buncher is drived by the klystron KIU-12 through a 28-dB directional coupler, located in between the pulse compression system and the AS. The average power, absorbed in the buncher is P_{ab}=2.9 W at pulse power of KIU-12 $P_0 \approx 13.8$ MW.

Accelerating section

The accelerating section of the prototype is the cylindrical disk-loaded waveguide with a constant impedance (constant geometry of cells along the AS, see fig. 4).

The section consists of 68 cells and 2 couplers which transform the basic waveguide mode TE_{10} to the accelerating mode of the section TM_{01} (see fig. 5).

In order to determine the dimensions of the section, cold tests of its cells were carried out. The experimental setup was assembled of 2 regular cells (one of it is for test) and 2 half-cells with emitting and receiving probes inside. By the results

of these tests cells with appropriate characteristics were selected and assembled on the special bench. To tune the AS, the measurements of reflection of an RF signal from the section and RF power dissipation in the AS were made. The section was matched with a waveguide to achieve the minimum reflection at the

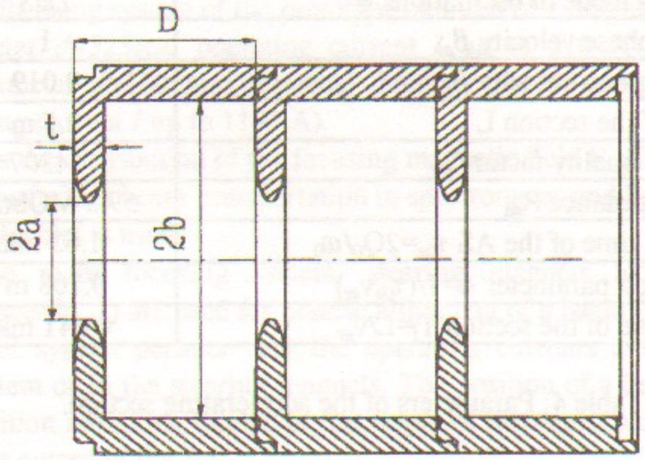

Fig. 4 Geometry of the AS cells.

operating frequency. Matching the coupler was done by adjusting the dimensions of the coupler input iris, diameter of the cavity and the size of a ring-shaped ledge around the beam channel to insure a low standing-wave ratio at the input

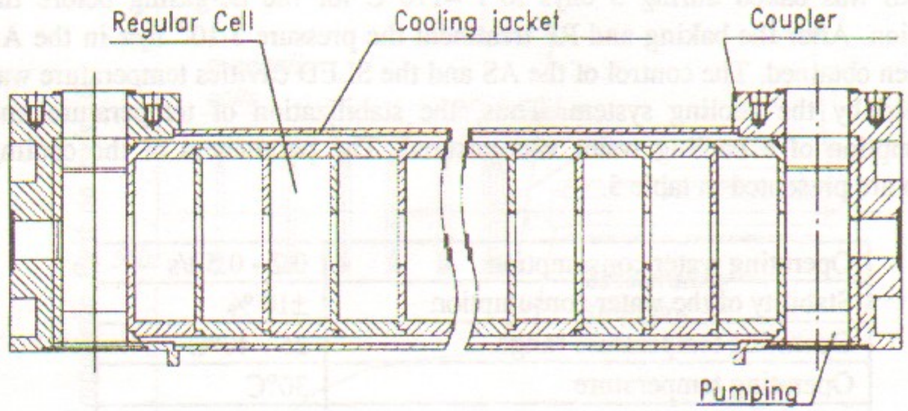

Fig. 5 General view of the AS.

and the output of the structure. The measurements were repeated after the AS brazing. The parameters of the section are presented in table 4.

Diameter of a cell 2b	84.4 mm
Iris aperture diameter 2a	24.0 mm
Iris thickness t	4 mm
Period D	35.7 mm
Operating mode of oscillations θ	$2\pi/3$
Relative phase velocity β_{ph}	1
Relative group velocity β_{gr}	0.019
Length of the section L	2.5 m
Unloaded quality factor Q_0	14307
Shunt impedance R_{sh}	59.3 MOhm/m
Unloaded time of the AS $\tau_{0a}=2Q_0/\omega_0$	1.63 mks
Attenuation parameter $\alpha=1/(\tau_{0a}v_{gr})$	0.108 m^{-1}
Filling time of the section $T_f=L/v_{gr}$	0.441 mks

Table 4: Parameters of the accelerating section.

When the average RF power at the AS input is P_{acc}=1.57 kW, the average power at the load input is equal to

$$P_l=P_{acc}e^{-2\alpha L} = 0.66 \text{ kW},$$

where α - attenuation parameter, L - length of section.
The average power dissipated in the AS

$$P_t=P_{acc}-P_l=0.91 \text{ kW}$$

The AS was baked during 3 days to $t \approx 170°C$ for the de-gasing before the operation. After the baking and RF treatment the pressure $3 \cdot 10^{-8}$ torr in the AS has been obtained. The control of the AS and the SLED cavities temperature was provided by the cooling system. Thus, the stabilization of temperature and consumption of a cooling water was ensured. The parameters of the cooling system are presented in table 5.

Operating water consumption	0.2 - 0.5 l/s
Stability of the water consumption	±10 %
Operating temperature range	25 - 40°C
Operating temperature	30°C
Allowable temperature variation	±0.1°C
Power consumption	Up to 20 kW

Table 5: Parameters of cooling system .

Beam transport system

The main focusing system of the prototype includes of 2 magnetic lenses, 6 ring coils (diameter d=525мм, operating current I up to 510 A) and a solenoid (internal diameter d=160 mm, external diameter D=320 mm, length L=2300 mm, operating current I up to 1100 A).

Fig. 6 shows the distribution of the focusing magnetic field B_z [G] along the prototype. For further beam transportation to spectrometer and Faraday cup, a quadrupole doublet is used.

Except the main focusing system, steering magnets located along the accelerator (see fig. 1) are used for precise alignment of a beam line.

The control system permits vary the operating currents either in the basic focusing system or in the steering magnets. The position of a beam is controlled by beam position monitors, located at the output of the thermionic gun and at the input and the output of the AS.

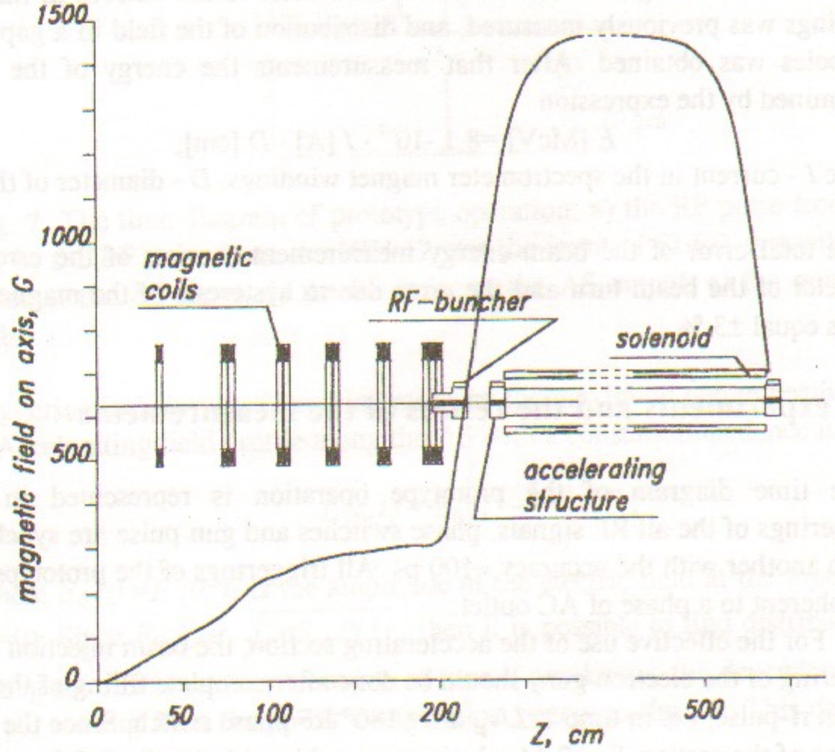

Fig. 6: The distribution of the focusing magnetic field.

Monitoring system

For the effective operation of the prototype the measurements of the energy characteristics of an accelerated beam and intensity of the bunch are required.

Measurements of the total charge of the bunch from the thermionic gun are produced by wall current monitor, located before the input of the buncher (see fig. 1).

The spectrometer is located downstream the AS and used to measure the beam energy and the energy spread in the bunch. The spectrometer utilizes a dipole magnet to steer the beam by 180°. When the magnet is not powered, the beam enters a straight-ahead line to Faraday cup, where bunch charge is measured.

The beam is spotted on the luminiscent screen at the spectrometer exit. Using the values of magnetic field H in the spectrometer, and diameter of beam turn D it is possible to determine the energy of accelerated electrons $\mathcal{E}=eHD/2$. By the size and relative brightness of the light spot on the screen one can estimate the energy spread in the bunch.

A ratio of the magnetic field in the spectrometer to the current in the magnet windings was previously measured, and distribution of the field in a gap between the poles was obtained. After that measurements the energy of the beam is determined by the expression

$$E\,[\mathrm{MeV}] = 8.1 \cdot 10^{-4} \cdot I\,[\mathrm{A}] \cdot D\,[\mathrm{cm}],$$

where I - current in the spectrometer magnet windings, D - diameter of the beam turn.

The total error of the beam energy measurement consists of the error in the diameter of the beam turn and the error due to hysteresis of the magnetic field, and is equal ±3 %.

The experiments and the results of the measurements

The time diagram of the prototype operation is represented in fig. 7. Triggerings of the all RF signals, phase switches and gun pulse are synchronized one to another with the accuracy ~100 ps. All triggerings of the prototype signals are coherent to a phase of AC outlet.

For the effective use of the accelerating section, the beam injection (the triggering of the electron gun) should be done after complete filling of the section by an rf-pulse, i.e. in time $\tau=L/v_{gr}$ after 180° RF phase switch. Since the filling time of the section $T_f \approx 0.44$ mks is comparable with the time of the signals propagation in supervising and control circuits, the moment of the electron gun

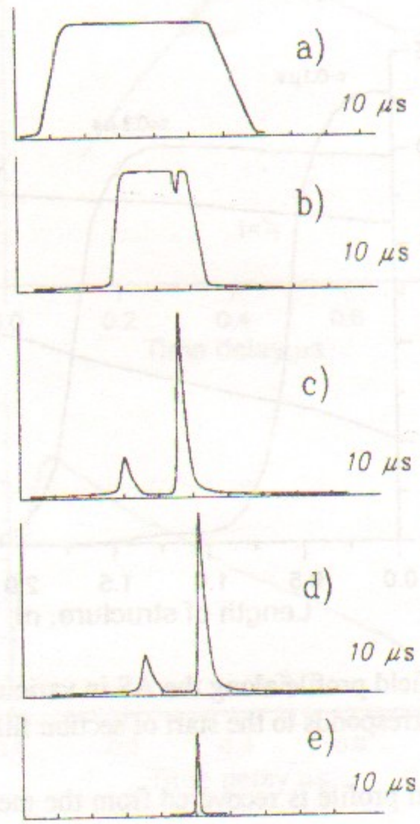

Fig. 7: The time diagram of prototype operation: a) the RF pulse from the KIU-37, b) the RF pulse from the KIU-12 (at the input of SLED system), c) the RF pulse at the AS input, d) the RF pulse at the AS output, e) the gun triggering pulse.

triggering is determined experimentally by the maximum output beam energy.

Accelerating field profile along the AS with a constant impedance is:

$$E(z,t) = E_0\left(t - \frac{z}{v_{rp}}\right)e^{-\alpha z},$$

where $E_0\,(t) = E\,(0,\,t)$ is the amplitude of the electric field at the input of the AS (z=0). Since $E_0\,(t) = \sqrt{2\alpha R_{sh} P(t)}$, then it is possible to find distribution $E\,(z,\,t)$ along the AS in various moments of time if one knows the dependence of power $P\,(t)$, coming from the power compression system to the AS. This distribution is shown in fig.8.

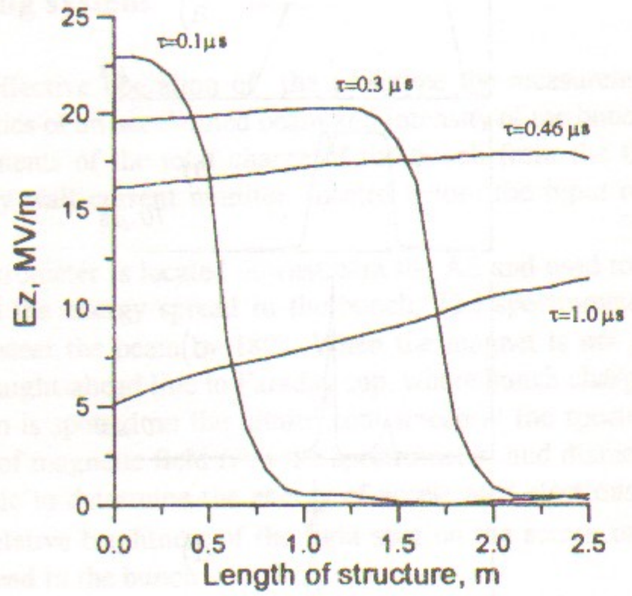

Fig. 8: Accelerating field profile along the AS in various moments of time. t=0 corresponds to the start of section filling.

The accelerating field profile is recovered from the measured pulse $P(t)$ at the input of the AS.

The maximum electric field in the input coupler of the AS (at z=0 and t=0) is E_0=24.5 MV/m. The accelerating gradient at $t=T_f$ is E_{acc}=17.7 MV/m. The choice of the SLED system parameters allow to provide the quasi uniform distribution of the accelerating field along the AS. Total beam energy gain as a function of the bunch transit time relative to the RF pulse τ is:

$$\mathcal{E}(\tau) = \int_0^L E(z,\tau)dz\ .$$

In fig. 9a the diagram of $\mathcal{E}(\tau)$ is shown. The dots on the diagram correspond to experimentally measured values. The good consent of experimental data with the theoretical analysis is obvious. Since the S-band buncher is powered by the same pulse as the section is, the RF power, coming into it at the moment of the bunch pass will also depends on τ. This dependence is presented in fig. 9b.

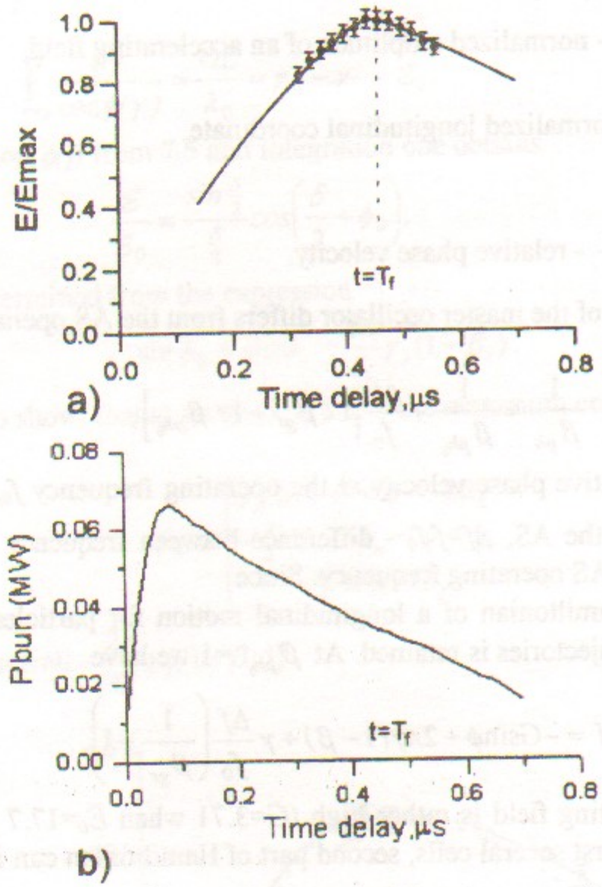

Fig. 9 a) The dependence of the beam energy gain on transit time delay (solid line - theoretical calculations),

b) The dependence of the buncher power at the moment of the bunch pass on time delay.

The acceleration of the beam occurs in a quasi uniform along the AS accelerating field. Therefore the basic energy dependencies could be obtained analytically. The equations of the longitudinal motion are

$$\frac{d\gamma}{d\xi} = G\cos\phi, \tag{7.1}$$

$$\frac{d\phi}{d\xi} = 2\pi\left(\frac{1}{\beta_{ph}} - \frac{1}{\beta}\right), \tag{7.2}$$

where $G = \frac{eEl}{mc^2}$ - normalized amplitude of an accelerating field,

$\xi = \frac{z}{l}$ - normalized longitudinal coordinate,

$\beta_{ph} = \frac{v_{ph}}{c}$ - relative phase velocity.

If the frequency of the master oscillator differs from the AS operating frequency, the

$$\frac{1}{\beta_{ph}} \approx \frac{1}{\beta_{ph_0}} + \frac{\Delta f}{f_0}\left[1/\beta_{gr} - 1/\beta_{ph_0}\right], \qquad (7.3)$$

where β_{ph_0} - relative phase velocity at the operating frequency f_0, β_{gr} - relative group velocity in the AS, $\Delta f = f - f_0$ - difference between frequency of the master oscillator and the AS operating frequency. Since
$G \approx const$, the Hamiltonian of a longitudinal motion for particles which move along the phase trajectories is retained. At $\beta_{ph_0} = 1$ we have

$$H = -G\sin\phi + 2\pi\gamma(1-\beta) + \gamma\frac{\Delta f}{f_0}\left(\frac{1}{\beta_{gr}} - 1\right). \qquad (7.4)$$

Since the accelerating field is rather high (G=3.71 when E_0=17.7 MV/m), after beam passes the first several cells, second part of Hamiltonian can is neglectable: when $\gamma \to \infty$

$$\gamma(1-\beta) \sim \frac{1}{2\gamma} \to 0.$$

Then it is possible to consider, the accelerating particles on the phase trajectories, determined by the equation:

$$\sin\phi \approx \sin\phi_i - \frac{2\pi}{G}\gamma_i(1-\beta_i) + \delta\frac{\gamma - \gamma_i}{\gamma_0 - \gamma_i}, \qquad (7.5)$$

where $\delta = \frac{2\pi L}{\lambda_0}\left(\frac{1}{\beta_{gr}} - 1\right)\frac{\Delta f}{f_0}$, L - length of the AS, λ_0 - operating wavelength, γ_i and ϕ_i - relative energy and phase of injected particles respectively, $\gamma_0 - \gamma_i = \frac{GL}{\lambda_0}$ - maximum kinetic energy gain in the AS at $f = f_0$. From the equation 7.1 one receives

$$\int_{\gamma_i}^{\gamma} \frac{d\gamma}{\cos\phi(\gamma)} = \frac{GL}{\lambda_0} = \gamma_0 - \gamma_i = \mathcal{E}_0. \qquad (7.6)$$

After substitution $\phi(\gamma)$ from 7.5 and integration one obtains

$$\frac{\mathcal{E}}{\mathcal{E}_0} = \frac{\sin\frac{\delta}{2}}{\frac{\delta}{2}}\cos\left(\frac{\delta}{2} + \phi_0\right), \qquad (7.7)$$

where ϕ_0 is determined from the expression

$$\sin\phi_0 = \sin\phi_i - \frac{2\pi}{G}\gamma_i(1-\beta_i)$$

It is possible to show, that at given G, γ_i and δ the maximum energy $[\mathcal{E}/\mathcal{E}_0]_{max}$ is reached at

$$\phi_0 = \begin{cases} \phi_x \text{ if } -\frac{\pi}{2} < \delta < -2\phi_x, \\ -\frac{\delta}{2} \text{ if } -2\phi_x < \delta < \pi, \\ -\frac{\pi}{2} \text{ if } \pi < \delta, \end{cases}$$

where $\phi_x = \arcsin[1 - \frac{2\pi}{G}\gamma_i(1-\beta_i)]$.

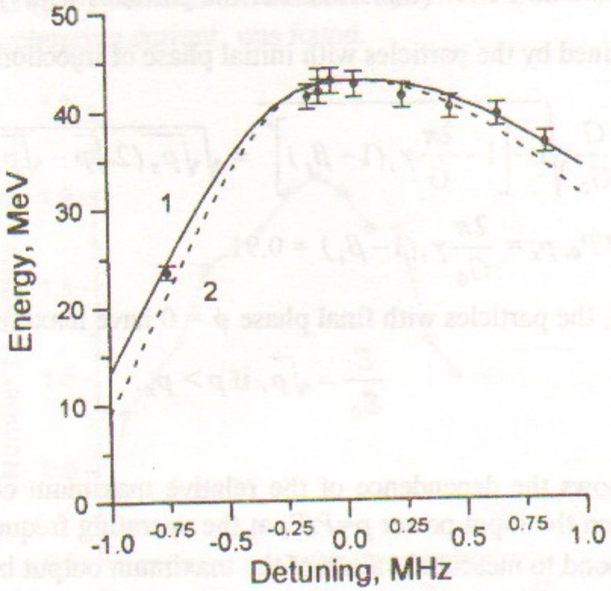

Fig. 10 The dependence of beam energy gain on the frequency detuning. 1 - computer simulation of the beam motion, 2 - analytical dependence, dots - experimental data.

Fig. 10 shows the maximum energy, gained by particles in the AS at G=3.71 and γ_i=1.2 (energy of injection 100 keV) vs. the value of the detuning $\Delta f=f-f_0$. The dots in the plot correspond to experimentally measured energies of the electron bunch. Curve 1 is the computer simulation of the beam motion using equations 7.1 and 7.2, curve 2 is the analytical dependence. The zero value of the detuning corresponds to $f_0 \approx 2798.3$ MHz, at which the maximum of accelerated bunch output energy is reached.

Since $G \sim E \sim \sqrt{P}$, where P is the driving power of the AS, it is possible, in the same assumptions of the high accelerating field, to find analytical dependence of the maximum output beam energy for various P. At Δf=0 one has

$$\mathcal{H} = -G\sin\phi_i + 2\pi\gamma_i(1-\beta_i) \approx -G\sin\phi.$$

Then

$$\frac{\mathcal{E}}{\mathcal{E}_0} = \frac{G}{G_0}\cos\phi = \frac{G}{G_0}\cos\left\{\arcsin\left[\phi_i - \frac{2\pi}{G}\gamma_i(1-\beta_i)\right]\right\}, \qquad (7.8)$$

where $\mathcal{E}_0 = \frac{G_0 L}{\lambda}$ = 44.3 MeV is the energy of the particles when the driving power $P = P_0$ = 28.5 MW (G_0=3.71). For the particles with $\mathcal{H} > 0$, the maximum energy is gained by the particles with initial phase of injection $\phi_i = \frac{\pi}{2}$, i.e.

$$\frac{\mathcal{E}}{\mathcal{E}_0} = \frac{G}{G_0}\sqrt{1-\left[1-\frac{2\pi}{G}\gamma_i(1-\beta_i)\right]^2} = \sqrt{\sqrt{p_x}(2\sqrt{p}-\sqrt{p_x})}, \text{ if } p < p_x,$$

where $p = P/P_0$, $p_x = \frac{2\pi}{G_0}\gamma_i(1-\beta_i) = 0.91$.

When $\mathcal{H} \le 0$, the particles with final phase $\phi = 0$ have maximum energy. So

$$\frac{\mathcal{E}}{\mathcal{E}_0} = \sqrt{p}, \text{ if } p > p_x.$$

Fig. 11 shows the dependence of the relative maximum output energy of the bunch $\mathcal{E}/\mathcal{E}_0$ on the input power $p=P/P_0$ at the operating frequency of the AS $f=f_0$. Dots correspond to measured values of the maximum output bunch energy. Curve 1 is the computer simulation of the beam motion using the equations 7.1 and 7.2, curve 2 is the analytical dependence.

In order to choose the optimum phase shift ϕ between the buncher and the AS the dependence of the accelerated beam current on the phase shift ϕ was measured. Fig. 12 shows dependence $I(\phi)$ at the AS operating frequency. The

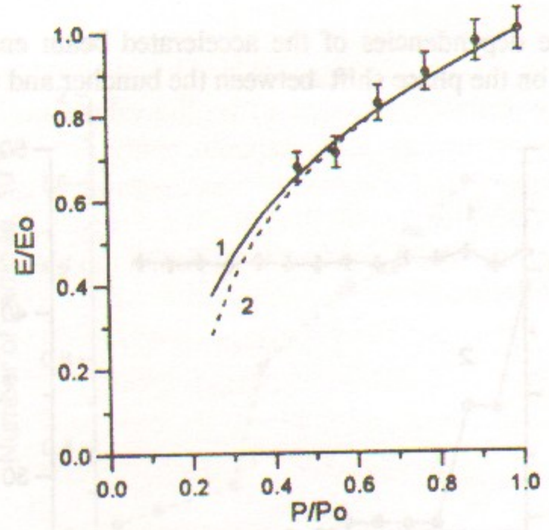

Fig. 11 The dependence of the relative output energy of the bunch on the input power. 1 - computer simulation of the beam motion, 2 - analytical dependence, dots - experimental data.

optimum phase shift (ϕ=0) between the buncher and the AS, which corresponds to the maximum accelerating current, was found.

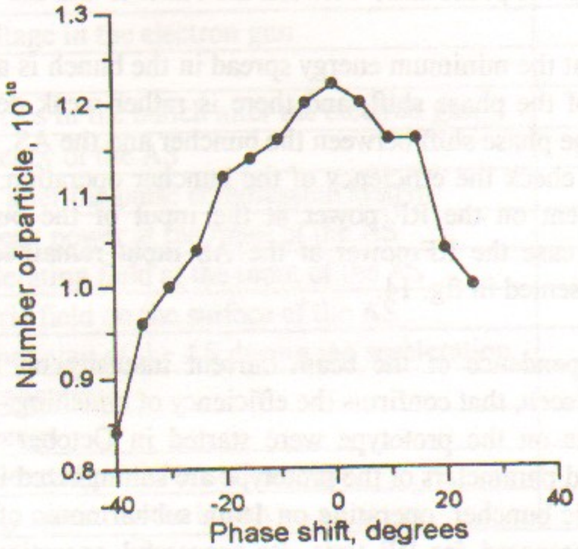

Fig. 12 The dependence of the accelerated beam current on the phase shift between the buncher and the AS (experimental data).

Fig. 13 shows the dependencies of the accelerated beam energy and energy spread in the bunch on the phase shift between the buncher and the AS.

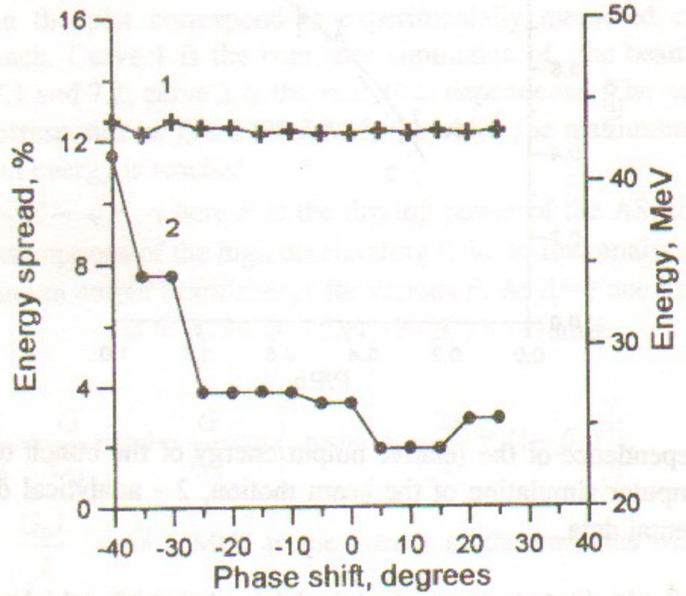

Fig. 13 The dependence of the accelerated beam energy (curve 1) and energy spread (curve 2) on the phase shift between the buncher and the AS.

It is obvious, that the minimum energy spread in the bunch is also reached near the chosen zero of the phase shift, and there is rather weak dependence of the beam energy on the phase shift between the buncher and the AS.

Besides this, to check the efficiency of the buncher operation, the dependence of the beam current on the RF power at the input of the buncher $I\ (P_{gr})$ is obtained. In that case the RF-power at the AS input remained constant. This dependence is presented in fig. 14.

Rather strong dependence of the beam current intensity on the field in the buncher is clearly seen, that confirms the efficiency of bunching.

The experiments on the prototype were started in October 1996. The most important achieved parameters of the prototype are summarized in tab. 6.

The subharmonic buncher, operating on 16-th subharmonic of basic frequency (174.8 MHz) is prepared for RF tests. Its successful operation will permit to check up the performance of the initial part of the preinjector in a single bunch mode.

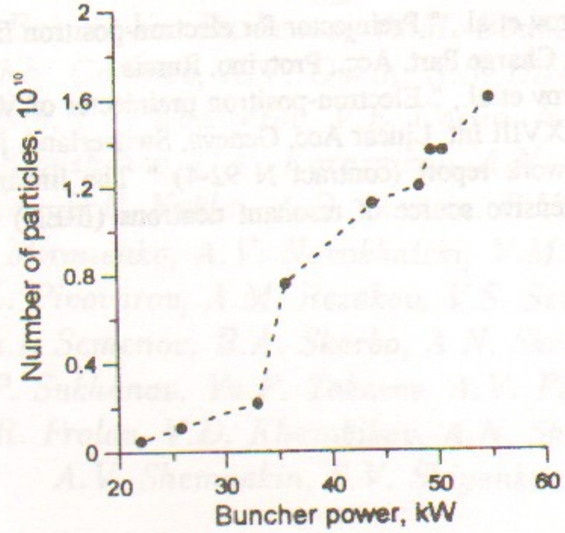

Fig. 14 The dependence of the beam current on the RF power at the input of the buncher.

Repetition rate	50 Hz
Accelerating voltage in the electron gun	100 kV
Bunch length	2.5 ns
Number of particles in the bunch after the electron gun	$5 \cdot 10^{10}$
Operating frequency of the AS	2798.3 MHz
RF pulse length after the pulse compression system	0.45 mks
Maximum RF peak power at the input of the AS	46.4 MW
Maximum accelerating field at the input of the AS	24.5 MV/m
Maximum electric field on the surface of the AS	49 MV/m
Peak power at the input of the AS during the acceleration	28.5 MW
Average acceleration rate	17.7 MeV/m
Output beam energy	44.3 MeV
Number of accelerated particles at the output	$1.2 \cdot 10^{10}$
Minimum energy spread in the bunch	± 1 %

Table 6: Parameters of the prototype.

References

[1] A.V. Aleksandrov et al., " Preinjector for electron-positron factories ". Proc. 1994 XIV Conf. On Charge Part. Acc., Protvino, Russia.
[2] A.V. Aleksandrov et al., " Electron-positron preinjector of VEPP-5 complex ". Proc. 1996 of the XVIII Int. Linear Acc. Geneva, Switzerland. Pp. 821-823.
[3] The research work report (contract N 92-4) " The linear accelerator of electrons for an intensive source of resonant neutrons (IREN) ", Novosibirsk, 1993, c.6-16.

A.V. Aleksandrov, M.S. Avilov, A.V. Antoshin,
P.A. Bak, O.Yu. Bazhenov, Yu.M. Boilmelshtein,
R.Kh. Galimov, K.V. Gubin, N.S. Dikansky,
A.G. Igolkin, I.V. Kazarezov, V.E. Carlin, N.A. Kisileva,
S.N. Klyushchev, O.V. Koroznikov, A.N. Kosarev,
N.Kh. Kot, D.E. Kuklin, A.D. Lisitsin, P.V. Logatchev,
L.A. Mironenko, A.V. Novokhatski, V.M. Pavlov,
I.L. Pivovarov, A.M. Rezakov, V.S. Severilo,
Yu.I. Semenov, B.A. Skarbo, A.N. Skrinsky,
D.P. Sukhanov, Yu.F. Tokarev, A.V. Filippov,
A.R. Frolov, V.D. Khambikov, A.N. Sharapa,
A.V. Shemyakin, S.V. Shiyankov

Test of the prototype of VEPP-5 preinjector

Budker INP 97-98

Ответственный за выпуск А.М. Кудрявцев
Работа поступила 3.12. 1997 г.

Сдано в набор 8.12.1997 г.
Подписано в печать 8.12.1997 г.
Формат бумаги 60×90 1/16 Объем 1.5 печ.л., 1.2 уч.-изд.л.
Тираж 120 экз. Бесплатно. Заказ N° 98

Обработано на IBM PC и отпечатано на
ротапринте ИЯФ им. Г.И. Будкера СО РАН,
Новосибирск, 630090, пр. академика Лаврентьева, 11.